Provisional chapter

Crystal Growth of Inorganic and Biomediated Carbonates and Phosphates

Antonio Sánchez-Navas, Agustín Martín-Algarra,
Mónica Sánchez-Román,
Concepción Jiménez-López, Fernando Nieto and
Antonio Ruiz-Bustos

Additional information is available at the end of the chapter

1. Introduction

Precipitation of carbonate minerals is tightly linked to water chemistry. After hydration of dissolved carbon dioxide, two pH-dependent partitioning-reactions govern the abundance of chemical species (H_2CO_3, HCO_3^- and CO_3^{2-}) formed in aqueous solution:[1,2]

$$H_2CO_3 \leftrightarrow HCO_3^- + H^+ \leftrightarrow CO_3^{2-} + 2H^+$$

where the O-H covalent bond in the oxyacid makes carbonate salts moderately soluble. The most common metal cations forming carbonate minerals are Ca^{2+}, Mg^{2+}, Mn^{2+}, Fe^{2+}, Pb^{2+}, Sr^{2+}, Co^{2+}, Ni^{2+}, Zn^{2+}, Cd^{2+} and Cu^{2+}. Continental and marine waters are enriched in Ca and Mg and are known to be saturated with respect diverse Ca-Mg carbonates such as calcite ($CaCO_3$), aragonite ($CaCO_3$) and dolomite ($MgCa(CO_3)_2$).[3] The concentration of the phosphate species (H_3PO_4, $H_2PO_4^-$, HPO_4^{2-}, and PO_4^{3-}) is also a function of pH, and their respective oxyacids are stronger than those of carbonic acids.[2] Because of this, phosphates are more stable than carbonates at low pH (<5). Chemical composition of phosphate minerals is more variable than that of carbonate minerals, and crystalchemical substitution of the PO_4^{3-} group by CO_3^{2-}, OH^-, F^-, Cl^-, etc, is rather common. In addition, numerous metals as Ca^{2+}, Mg^{2+}, Fe^{2+}, Na^+, Sr^{2+}, Ce^{3+}, La^{3+}, Ba^{2+}, and Pb^{2+} can be incorporated into the structure of the phosphate minerals.

Limestones and dolostones constitute the most important carbonate reservoirs on the Earth, but phosphates are much more diluted within the Earth crust, as phosphate rocks are much

less common that carbonate rocks. Nevertheless, many organisms form $CaCO_3$ shells, and Ca-carbonates and phosphates are the main constituents of normal bone and of pathologically calcified organic tissues.[4] In many cases, the precipitation of carbonate and phosphate minerals at Earth-surface conditions is a organic matrix- biomediated process related to shell formation. Indeed, carbonate and phosphate crystals form sophisticated composite materials (*e.g.*, shells, spicules, bones, teeth), where they appear embedded within an organic framework, which apparently controls the final texture of the mineralized material. When these organisms die, Ca-carbonate shells accumulate to form limestone. Precipitation of Ca-carbonate often occurs in domestic and industrial installations where untreated natural waters are used.[5]

The study of the origin of life on Earth, and of the possible existence of extraterrestrial life is also tightly associated with carbonate and phosphate precipitation, as it is recorded in microbial accretions, frequently forming stromatolites and oncoids.[6-9] Ca- and Mg- carbonate and phosphate minerals similar to those found in ancient and modern stromatolites are also usually obtained in laboratory bacterial culture experiments.[10-13]. The occurrence of amazing complex textural features in relation to these minerals in the geologic record has prompted many authors to consider them as biomarkers.[14]

Different formation mechanisms have been proposed for bacterially mediated carbonate and phosphate minerals.[15] The metabolic activity of the bacteria alters the physico-chemical parameters of their surrounding habitats, allowing mineral precipitation. It has been suggested that microbes influence nucleation and that, in general, they control the kinetics of precipitation of carbonate and phosphate minerals, and therefore their morphology. Spheroidal precipitates (spherulitic bioliths) are commonly obtained in bacterial culture experiments.[13]

Some crystal-growth studies have shown that the microstructure of carbonates and phosphate minerals precipitated by bacteria at high supersaturation conditions has particular signatures.[7,13,16] They nucleate as nanocrystal units after the precipitation of amorphous precursors, and then, start to grow, developing spherulites and dumbbells. Singular crystal-growth features of aragonite and calcite occur in diverse species of molluscs as result of the inhibition of growth of specific crystallographic faces by organic molecules. [17] However it is well known that the habit of the crystals formed at high supersaturation is completely different from the crystal growth features observed in precipitates obtained at lower supersaturation.[18] Hence, spheroidal morphology may results from different origin. In addition, some crystal aggregates that normally occur in shells can be easily explained by competitive crystal growth processes.[17]

In this chapter, we describe similar crystal growth features in inorganic and biogenic carbonates and phosphates formed in natural environments and in laboratory experiments. We focus on the importance of the kinetics on the crystal habit of carbonates and phosphates precipitated in biological and abiotic systems. We also discuss the influence of the nature and composition of the precipitation medium, as well as the structural control on crystal habit of Ca-Mg carbonates.

2. Material and methods

2.1. Natural Ca-phosphate samples

Crystal growth studies of natural Ca-phosphate have been performed on ancient phosphate stromatolites and on modern calcified tissues. Stromatolites come from Upper Jurassic and Lower Cretaceous limestones of the Betic Cordilleras, Southern Spain (Almola Sierra and Peñón del Berrueco, respectively). Calcified tissues correspond to enamel, dentine and bones from laboratory rats.

2.2. Inorganic experiments

The inorganic synthesis of amorphous calcium phosphate was obtained mixing 300 ml of 0.04 M calcium salt ($CaCl_2.6H_2O$) with 0.036 M ammonium phosphate dibasic salt ($(NH_4)_2HPO_4$) in 400 ml of constantly stirred 0.15 M buffer. All solutions were thermally equilibrated at 25ºC before mixing. The amorphous precursor phase was removed immediately after mixing.

Inorganic growth of carbonates in laboratory experiments was performed by using aqueous solutions of diverse metal cations (mainly Ca^{2+}, Mg^{2+}, Fe^{2+} and Pb^{2+}) and carbon dioxide or highly soluble bicarbonate/carbonate salts as source for carbonate ions. Inorganic solution growth of carbonates was carried out by bulk crystallization (free drift experiments), where two solutions of relatively easily dissolved salts of the diverse metals and sodium bicarbonate/carbonate were mixed: $Pb(CH_3COO)_2.3H_2O$, $CaCl_2.6H_2O$, $Ca(NO_3)_2.4H_2O$, $MgCl_2.6H_2O$, $FeCl_3.6H_2O$, $Fe(ClO_4)_2.nH_2O$, Na_2CO_3 and $NaHCO_3$ (see results for the specific concentrations used for the precipitation of the different obtained carbonate minerals). The resulting solution becomes supersaturated with respect to the less soluble metal carbonate. Temperature was usually 25ºC. Gel growth of Ca-Mg carbonates was performed by the counter-diffusion of carbonate solutions versus solutions containing diverse metal salts through a column of silica gel (stock solutions, 1 M of Na_2CO_3, 1 M $CaCl_2.6H_2O$, and variable concentrations of $MgCl_2.6H_2O$; see below). The silica gel with a pH 5.5 was prepared by acidification of sodium silicate solution with 1 M HCl. It was poured into a U-tube and allowed to polymerize to a solid gel.

2.3. Bacterially mediated precipitation

A liquid culture medium with a natural bacterial consortium mainly belonging to the genus *Acetobacter* sp., was used for biomediated precipitation of Ca, Fe and Pb phosphates and carbonates. This consortium was obtained from vinegar dregs after natural degradation of untreated wine. Aerobic *Acetobacter* grown in wine makes volatile acetic acid in the form of vinegar, and oxidizes acetic acid to carbon dioxide and water. Bacteria metabolize nitrogenated organic matter (*e.g.* proteins) with the subsequent production of CO_2 and NH_3. Metal cations were added to the liquid culture as soluble salts (50 mM $CaCl_2.6H_2O$, 50 mM $FeCl_3.6H_2O$ and 5 mM $Pb(NO_3)_2$) to obtain phosphate and carbonate minerals. Yeast extract (1%) was the carbon source for bacteria growth.

Concerning phosphate, bacterial phosphate precipitates of Fe and Pb were obtained, but with only minor amounts of lead phosphate, since bacterial tolerance to Pb is very low. Concerning carbonates, NH_3 production by *Acetobacter* increases the basicity of the precipitating medium (thus favouring the formation of carbonate minerals) but vinager acidity obviously hinders carbonate precipitation. So the culture medium was supplemented with bicarbonate (50 mM $NaHCO_3$), and the pH adjusted to 5.5-6 with 1 M NaOH to favour the precipitation of Ca-carbonates.

2.4. Analytical techniques

Natural mineral samples and laboratory precipitates (both biotic and inorganic) were analyzed by X-ray-diffraction (XRD) using a PANalytical X'Pert Pro diffractometer (CuKα radiation, 45kV, 40mA) equipped with an X'Celerator solid-state lineal detector and on line connection with a microcomputer. The diffraction patterns were obtained by using a continuous scan between 3-50 º2θ, 0.01 º2θ of step size and 20 s of time step. Data processing was performed using Xpowder®.[19]

Carbonates and phosphates were studied with a high-resolution Field-Emission Scanning Electron Microscope (FESEM) LEO GEMINI 1525, equipped with an energy dispersion X-ray (EDX) spectroscopy microanalysis Inca 350 version 17 Oxford Natural samples and inorganic (abiotic) and bacterial (biotic) precipitates were studied under Transmission Electron Microscopy (TEM). Representative samples of the natural material (stromatolites and calcified tissues) were ion-milled after extraction from selected areas of thin sections. The same powder samples of bacterial and inorganic precipitates used for XRD analyses were embedded in an epoxy resin, then sectioned by ultramicrotome following the methodology of Vali and Koster for clays,[20] and finally carbon coated. The samples were examined using a LIBRA 120 PLUS EFTEM (Energy Filtered TEM) instrument equipped with in-column corrected OMEGA Filter, operating at an acceleration voltage of 120 kV. Optimum amplitude contrast was achieved using lens aperture of 30 mm, and afterward removing inelastic electrons by zero-loss filtering in the elastic scattering image (ESI) mode. Electron energy loss spectroscopy (EELS) was also performed with this instrument. HRTEM and analytical electron microscopy study was performed using a Philips CM20 instrument (Philips) operated at 200 kV and equipped with an EDX system EDAX for microanalysis.

3. Results

3.1. Crystal growth features in phosphate stromatolites and calcified tissues

Ca-phosphate mineral occurring in stromatolites is francolite ($Ca_5(PO_4)_{2.5}(CO_3)_{0.5}F$). Francolite is a low crystalline variety of apatite.[7,21] XRD analyses show that francolite from phosphate stromatolites is more crystalline than other phosphate minerals precipitated by us in the laboratory (Fig 1). Secondary electron images of the phosphate stromatolites show the occurrence of accretion structures with columnar and arborescent morphologies defined mainly by francolite (Fig. 2A). Phosphate laminae alternate with particulate sediment layers,

and appear surrounded by a sediment matrix. These sediments are made of cryptocrystalline carbonate (micrite) formed by bioclastic particles (Figs. 2B-C). Sediment particles were trapped by microbes (heterotrophic bacteria) within the biosedimentary structure. Gelly-like appearance of arborescent morphologies and other mineralized structures, such as tubular bridges with smooth surfaces connecting phosphatic microcupolae (Figs. 2C and 2D), constitute the fossil microbial mat.

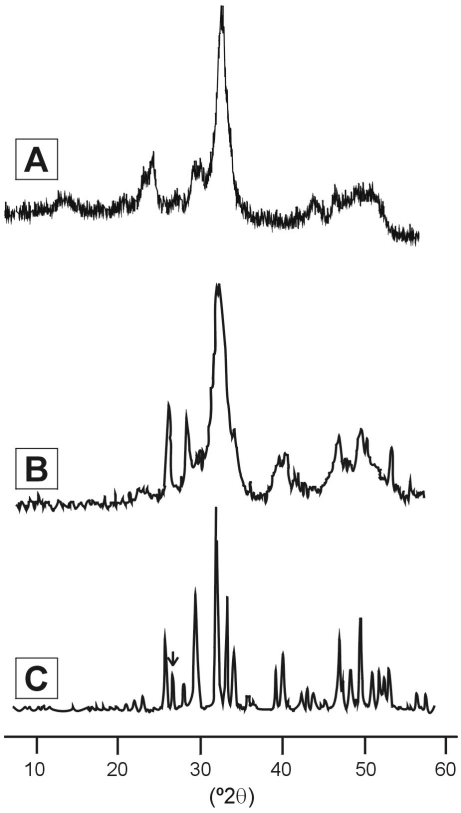

Figure 1. XRD patterns corresponding respectively to Pb-phosphate from biomediated laboratory experiments (A), Ca-phosphate from inorganic precipitates (B) and Ca-phosphate from phosphate stromatolites (C). Arrow in figure C corresponds to quartz.

The authigenic laminae within stromatolites are defined by the occurrence of neoformed minerals containing P, Fe, Mn and Al, as deduced from X-ray maps of figure 3. Amorphous precursors of francolite, calcite, iron oxyhydroxides and clay minerals, mainly smectites are still preserved in small areas within these authigenic laminae as evidenced in TEM images (Figs. 4 and 5). The authigenic minerals within microbial laminae normally surround sediment particles such as terrigenous grains (detrital clay and quartz), micron-sized fossils (benthic and

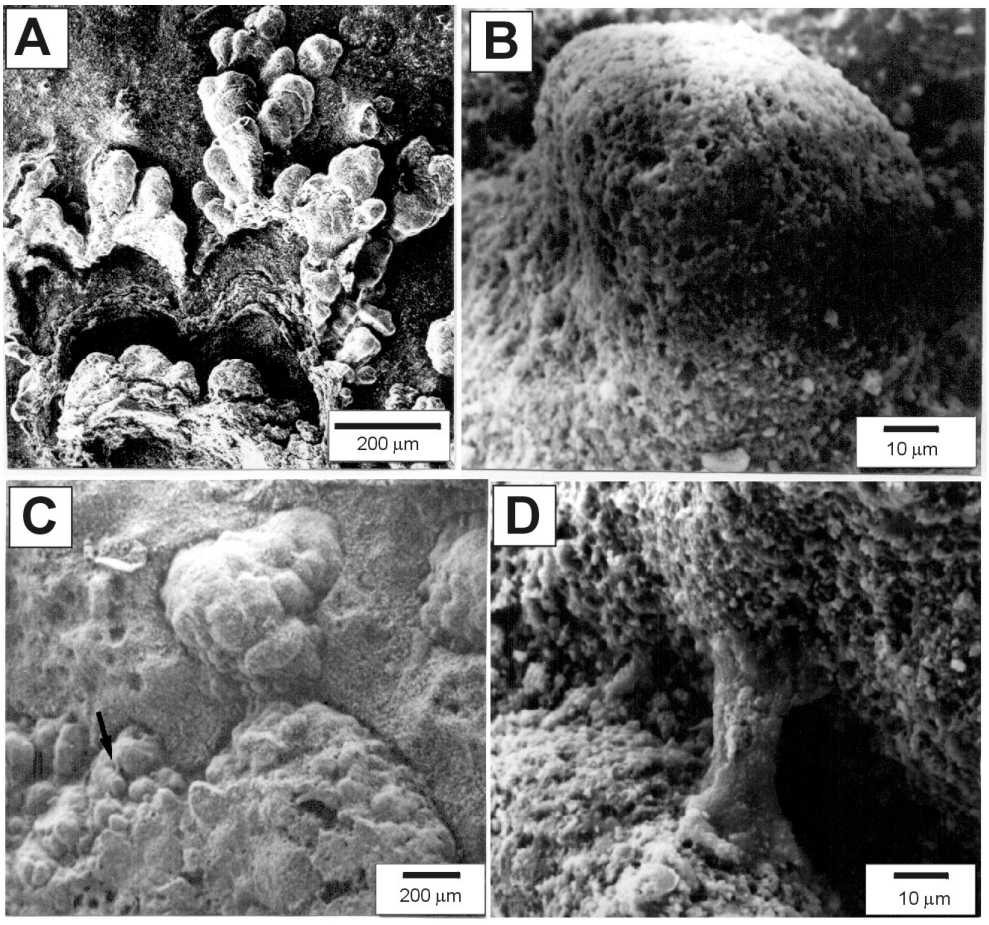

Figure 2. Secondary electron images from phosphate stromatolites. (A) General view of arborescent microstromatolites (etched sample). (B) Cupola formed by francolite. (C) Carbonate-rich sediment located among the phosphate cupolas (arrow points to close-up shown in D). D) Gelly-like tubular bridge between two phosphate domes; it is made of poorly crystalline P-rich and Si-Al-Fe-rich substances.

plancktonic foraminifera and coccoliths) and bioclasts that constitute the fine-grained marine, mainly carbonate sediment (Fig. 5). Francolite crystals from these laminae are nanometre-sized prisms with hexagonal basal sections and elongated along the *c* axis. Lattice fringes at 0.8 nm are observed (Fig. 4A).

Crystal growth features described for francolite in stromatolites are very similar to those observed for Ca-phosphates from calcified tissues (enamel, dentine and bone), which mainly correspond to hydroxyapatite. Dentine from adult rats shows accretion patterns defined by alternating layers composed by hydroxyapatite crystals and collagen fibrils (Fig. 6A). Honey-

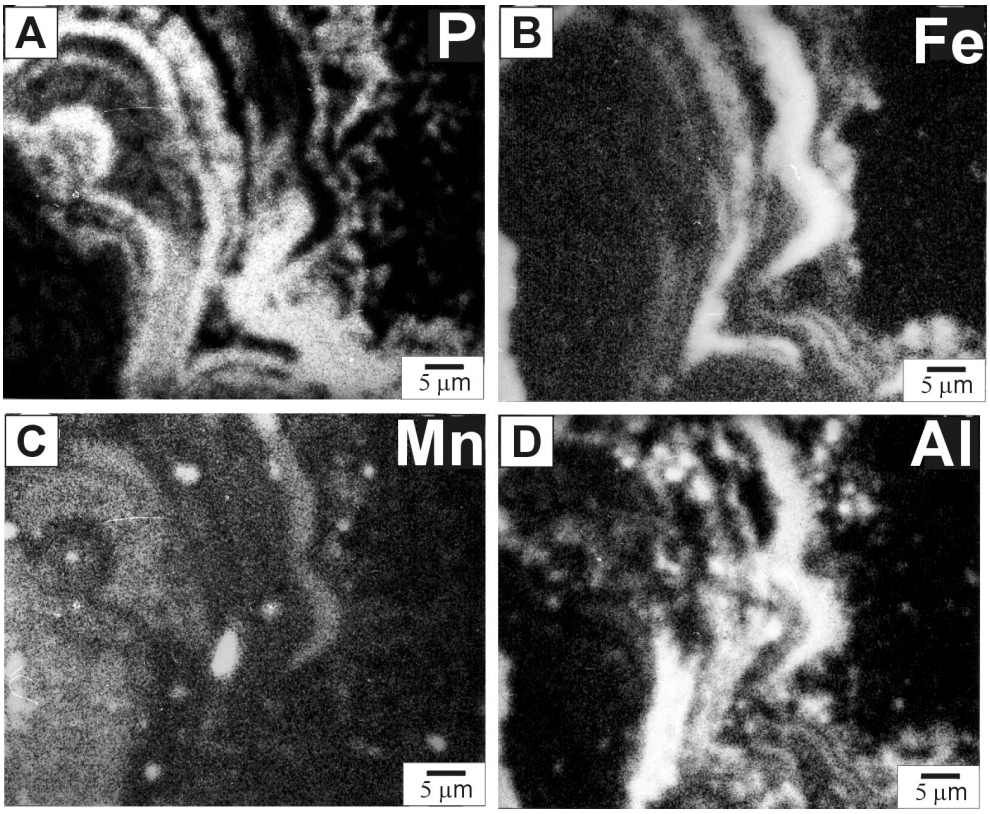

Figure 3. X-ray images of P (A), Fe (B), Mn (C) and Al (D) defining lamination in stromatolites. P-rich laminae are made of francolite. Fe- and Mn-rich laminae correspond to Fe and Mn oxyhydroxides, respectively. Authigenic and detrital clays are represented by the Al-rich areas. Most black areas in these images correspond to carbonate sediment, which is mainly calcite.

comb-like aggregates of small hexagonal apatite crystals of dental enamel (Fig. 6B) are roughly equivalent to parallel aggregates of prismatic phosphate crystals observed in phosphate stromatolites (Fig. 7 in Sánchez-Navas and Martín-Algarra).[7] Hydroxyapatite crystals in dentine have lower sizes than in enamel, and appear embedded in an organic framework (Fig. 7). They are usually closely packed in subparallel aligments, with the long dimension *c* axis being attached to collagen fibrils.[23,24]

Precursory phases of the Ca-phosphate have been observed in the studied calcified tissues, as evidenced by TEM images corresponding to the incipient stages of mineralization in dentine, enamel and bone of young rats and embryos (Fig. 8). In the case of enamel from embryos, amorphous calcium phosphate forms rounded masses of more electron dense material within an organic matrix (Fig. 8A). Nanometre-sized acicular crystals can be differentiated from amorphous Ca-phosphate forming electron dense regions with massive texture in TEM

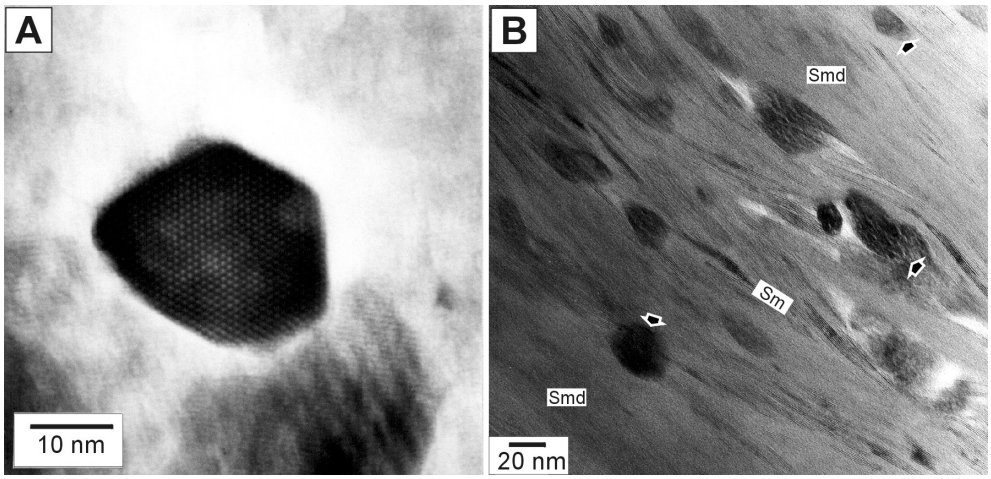

Figure 4. (A) HRTEM image of a francolite nanocrystal from an authigenic phosphate stromatolite lamina. It corresponds to a (001) hexagonal basal section. Three equivalent sets of crystallographic planes can be observed: (100), (010) and (110), intersecting at 120º, with an interplanar spacing of 0.82 nm. (B) Spindle-like packets 20-50 nm thick of smectite (Sm) with layer terminations and wavy layers from the same stromatolite lamina as A. Packets without fringe contrast (Smd) result from slight misorientation of the layers, mostly with 1 nm *d*-spacing. Fe-rich amorphous substances (arrows) are intergrown between smectite packets.

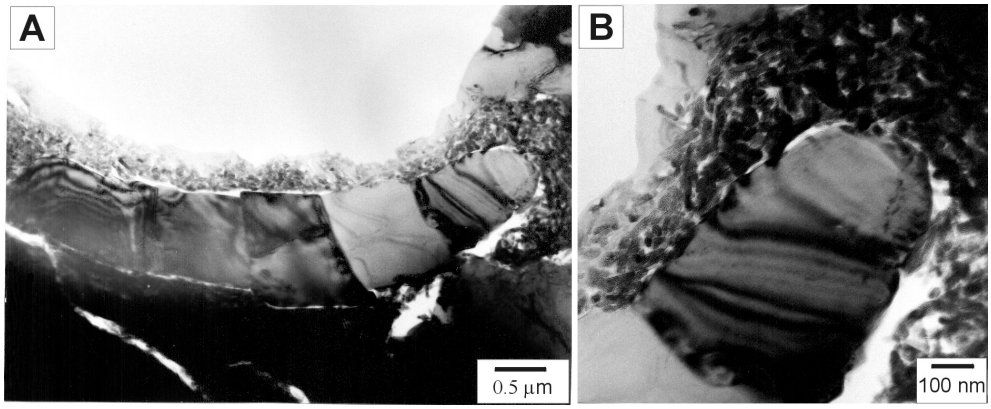

Figure 5. (A) TEM image of a coccolith bioclast surrounded by iron oxyhydroxides within an authigenic phosphate stromatolite lamina (compare this image with the transmission electron micrographs of cocoliths of Figure 17 in de Vrind-de-Jong and de Vrind, 1997).[22]. This bioclast is made of five calcite crystals, each around 1μm in size. (B) Detail of iron oxyhydroxide nanocrystals surrounding the bioclast. The average diameter of these crystals is 30 nm in pseudo-hexagonal sections, and around 70 nm along directions perpendicular to basal section.

images; this is particularly evident in dentine (Figs. 8B and C), and in bone from one-day-old rats (Fig. 8D).

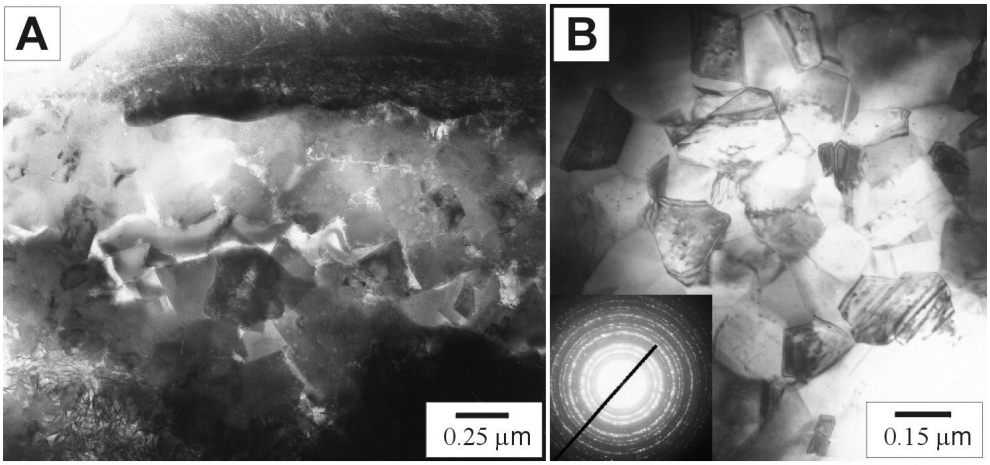

Figure 6. (A) TEM image of hydroxyapatite crystals surrounded by collagen fibrils in dentine from adult rat. (B) Honeycomb-like aggregate of small hexagonal crystals (50–200 nm in average size) in dental enamel of adult rat. Note the concave-convex boundaries among crystals. Inset corresponds to selected area diffraction pattern of the parallel aggregate of hydroxyapatite crystals with their *c* axis parallel aligned to the normal to outer surface.

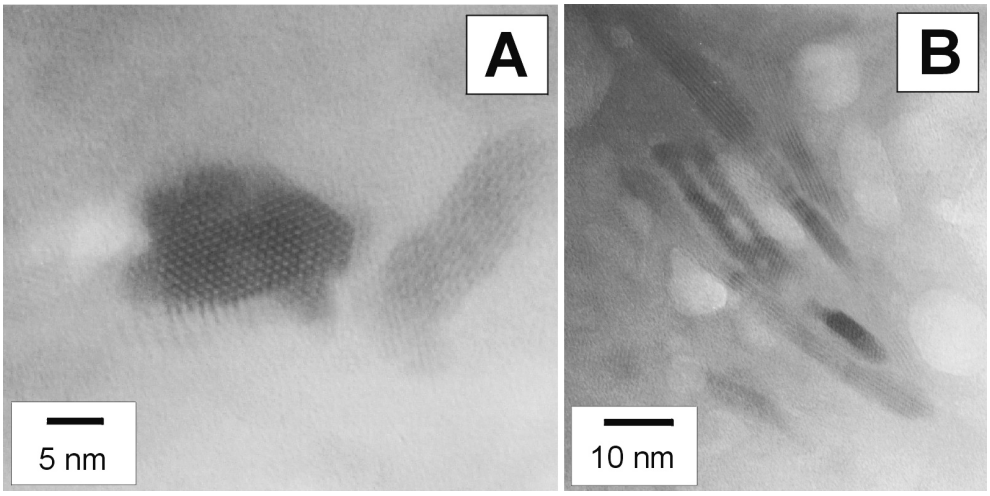

Figure 7. HRTEM images of nanocrystallites of hydroxyapatite in dentine. Crystals appear oriented with their *c* axis normal (A) and parallel (B) to the plane of observation. Lattice-image of figure A corresponds to a hexagonal section of one nanocrystal, for which the three sets of equivalent lattice planes parallel to *c* axis, with interplanar spacings at 0.82 nm, are resolved simultaneously. Crystals have sizes around 10-15 nm in basal section (A) and up to 80 nm in length following the *c* axis (B).

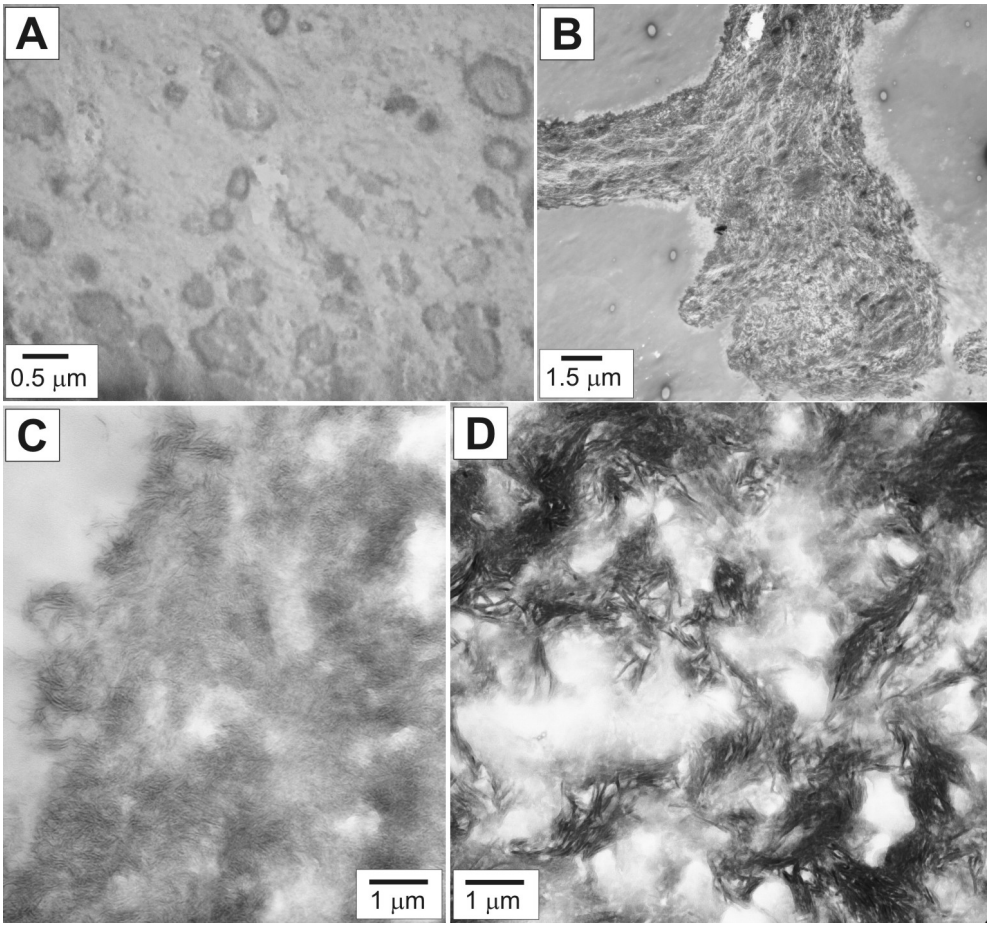

Figure 8. TEM images showing incipient mineralization of hard tissues. (A) Amorphous calcium phosphate forming electron dense masses within a lower electron dense organic matrix in enamel from rat embryo. (B) Electron dense regions formed by amorphous calcium phosphate in dentine from one-day-old rat. (C) Magnified TEM image showing thin nano-sized crystals within the mineralized regions shown in (B). (D) TEM image (ESI mode) needle-shaped crystals in bone from one-day-old rat.

3.2. Inorganic phosphate and carbonate minerals obtained by solution and gel growth

Poorly crystalline Ca-phosphates have been determined after XRD study of inorganic precipitates (Fig. 1B). In the secondary electron images they appear as clumps with a foamy porous structure, where nanometre-sized acicules are visible in the most crystalline areas (Fig. 9A). TEM images confirm the existence of needle-shaped crystallites, which normally appear surrounded by structureless films and "clouds" of amorphous calcium phosphate (Fig. 9B). The acicular crystals are up to 30 nm in length and up to 4 nm in thickness. In some cases,

lattice fringes at 0.8 nm corresponding to *d*-spacing of (100) crystallographic planes of apatite are observed (Fig. 9C). There exists a marked resemblance between these TEM images and those previously shown for calcified tissues in one-day-old rats (Figs. 8B-D). Thus, needle-shaped Ca-phosphate nanocrystals surrounded by amorphous calcium phosphate occur both in the non-mature bone (Fig. 8D) and in the inorganic precipitates (Fig. 9C).

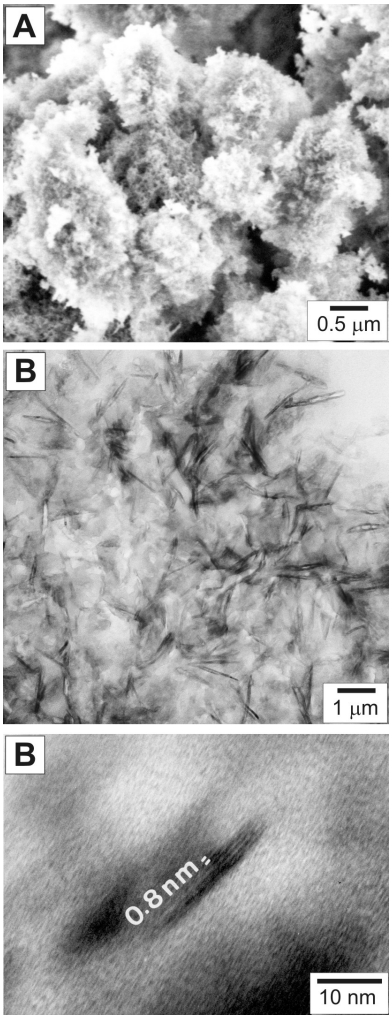

Figure 9. (A) FESEM image of inorganically precipitated phosphate sample showing structureless "clouds" of amorphous calcium phosphate including acicular crystals. (B) ESI-mode TEM image of the inorganically precipitated phosphate sample, where nano-sized needle crystals of apatite are included within amorphous calcium phosphate. (C) Lattice-fringe image of needle apatite crystallite with lattice fringes at 0.82 nm corresponding to the *d*-spacing of (100) or equivalent crystallographic planes.

Rhombohedral micron-sized siderite ($FeCO_3$) crystals and siderite spherulites have been precipitated in oxygen-free water inside an anaerobic chamber from solutions with salt concentrations 50 mM $NaHCO_3$–50 mM $Fe(ClO_4)_2.nH_2O$ and 1 M $NaHCO_3$–1 M $Fe(ClO_4)_2.nH_2O$, respectively (Fig. 10). Siderite spherulites normally show rough surfaces formed by uniaxial aggregates of skeletal crystals with nanometre size (Figs. 10C and D). Both siderite crystals and spherulites appear surrounded by a poorly-crystalline precursory material formed by iron oxyhydroxides (Figs. 10E and 10F).

Crystallization of Ca-Mg rhombohedral carbonates were conducted through gel-growth experiments to favour the incorporation Mg to the calcite structure. The effect of Mg content on the structural parameters and on the crystal habit of calcite was analyzed. Thus, calcite rhombohedrons with dendritic morphologies were formed in Mg-free crystallization experiments (Fig. 11A). Calcite crystals with rough surfaces and crystal morphologies corresponding probably with {021} forms (Fig. 11B) and calcite spherulites (Fig. 11C) grew from 0.1 M and 1 M $MgCl_2.6H_2O$ stock solutions, respectively. The increase of the Mg-content also produced a lattice contraction and a decrease of the crystallinity of the Ca-Mg carbonate, as well as the appearance of metastable phases (monohydrocalcite) as deduced from XRD analyses (Fig. 11D).

Spherulites composed by low-crystalline Mg-rich Ca-Mg carbonates were also studied by SEM and TEM. Secondary images of these spherulites indicate that they grew by adhesion of nanometre-sized particles (Fig. 12A). In addition, TEM study of these samples reveals the occurrence of carbonate nanocrystal building units, with sizes from 40 to 80 nanometres in diameter, which aggregate to form small clusters with approximately the same crystallographic nanocrystals orientation (Fig. 12B).

3.3. Crystal growth features of bacterially-mediated phosphates and carbonates

Bacterially-mediated phosphate and carbonate precipitates show analogous crystal growth features to those of some inorganic (abiotic) precipitates (compare Figs. 10B, 11A and 12A with Figs. 13 and 14). Poorly crystalline Fe- and Pb-phosphates occur in relation to bacterial cells, organelles and biofilms during the initial stages of biomineralization (Figs. 13A and 13B).

Fe-phosphate spherulites and capsules with diverse sizes and textural features were formed after several weeks (Figs. 13C-13E). Voids and channels with widths of 200 nanometres and 1 micron in length are normally observed in SEM images of Fe-phosphate spherulites (Figs. 13C and 13D). Fe-phosphate capsules develop a central hollow (Fig. 13E).

Other bacterially-mediated precipitates are constituted by poorly crystalline Pb-phosphates (Fig. 13F). Their low crystallinity is evidenced by the broad peaks observed in the XRD patterns (Fig. 1A). Secondary electron images obtained from of *Acetobacter* Pb cultures show two different types of precipitates (Fig. 13F). Those of largest dimension correspond to Pb-phosphate spherulites. The smallest precipitates are constituted by irregular clumps of spheroidal Pb carbonates (hydrocerussite) particles around 0.1-0.3 μm in diameter, formed by aggregation of nanoparticles.

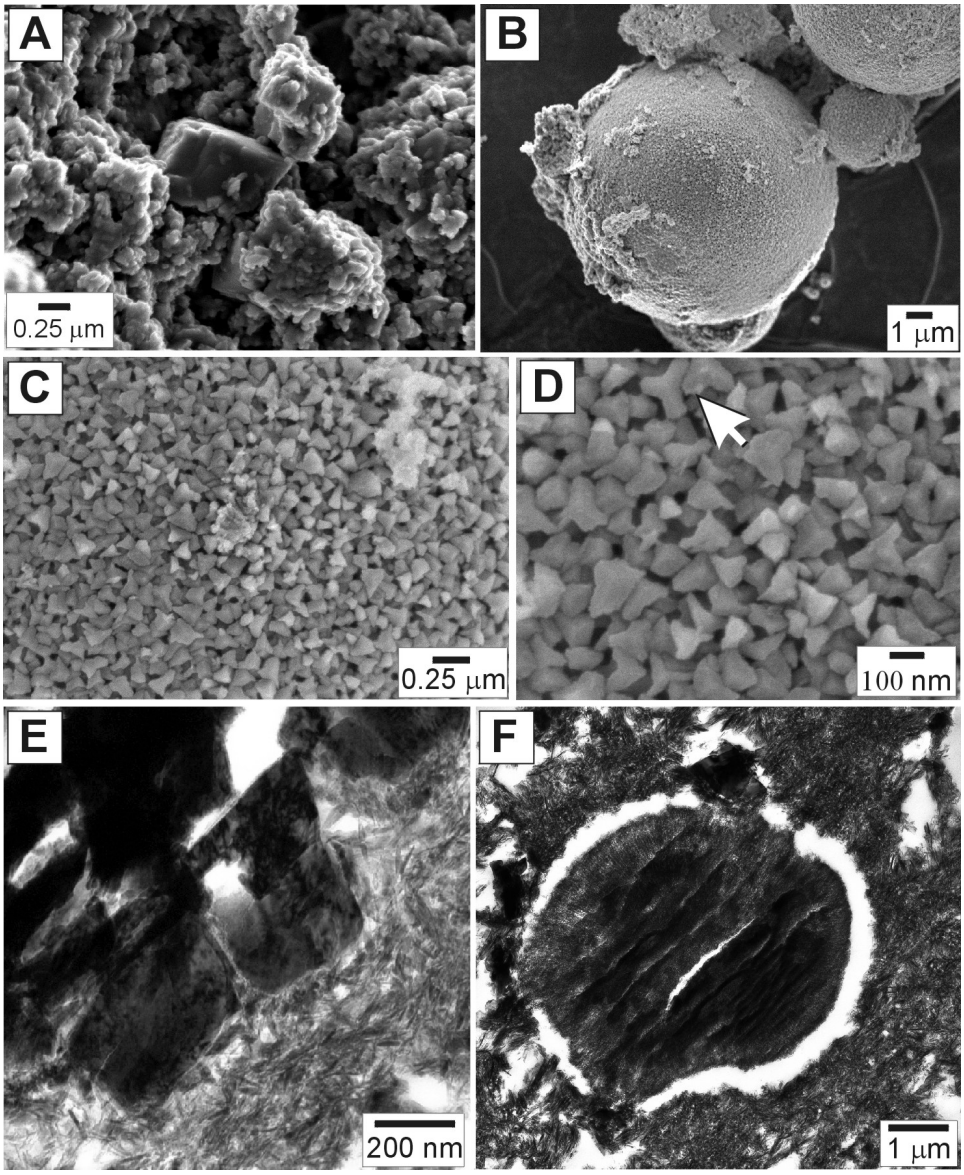

Figure 10. (A) Secondary electron image of siderite rhombohedron surrounded by less crystalline precipitates obtained from solution growth at the following salt concentration: 50 mM $NaHCO_3$, and 50 mM $Fe(ClO_4)_2.nH_2O$. (B) Siderite spherulites partially covered with a thin poorly crystalline Fe-rich layer obtained from solution growth at the following salt concentration: 1 M $NaHCO_3$, and 1 M $Fe(ClO_4)_2.nH_2O$). (C) Uniaxial aggregate of crystals at the rough surface of a siderite spherulite. (D) Close-up of (C) showing the triangular tips of the tripod-like dendritic crystals of siderite. (E) TEM image of rhombohedral siderite crystals surrounded by small needle-like iron oxyhydroxydes. (F) TEM view of a siderite spherulite within a poorly crystalline Fe-rich matrix.

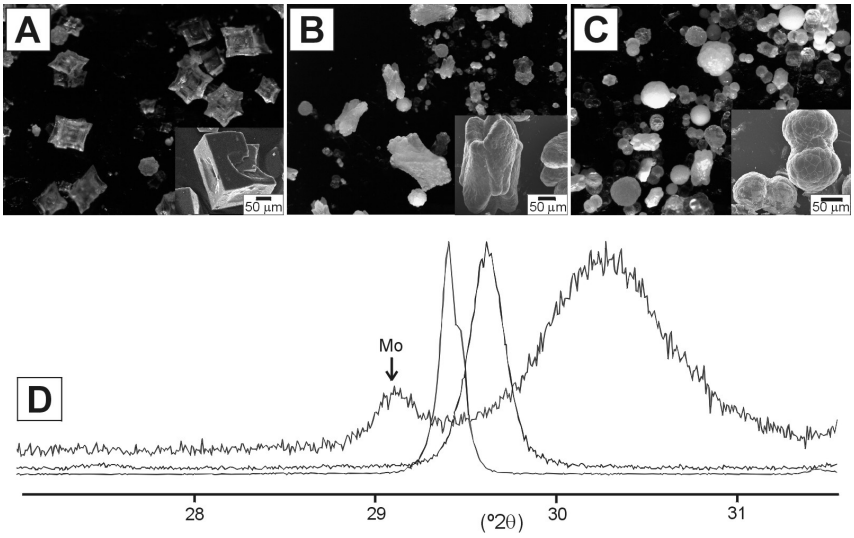

Figure 11. (A) to (C): Optical images and SEM views (insets) of the Ca-Mg carbonates obtained from gel growth inorganic precipitation experiments. (D) XRD features of their (104) peaks. (A) Dendritic calcite crystals precipitated in Mg-free medium. (B) Crystal morphologies of magnesian calcites precipitated from 0.1 M $MgCl_2.6H_2O$ stock solution. (C) Spherulites formed in Mg-richest medium (1 M $MgCl_2.6H_2O$ stock solution). (D) XRD patterns showing the displacement and broadening of the (104) peak with increasing Mg content of the Ca-Mg carbonate from calcite (A) to Mg-calcite (B) and to Mg-kutnahorite (C). Monohydrocalcite (Mo) is also formed together with the Mg-kutnahorite.

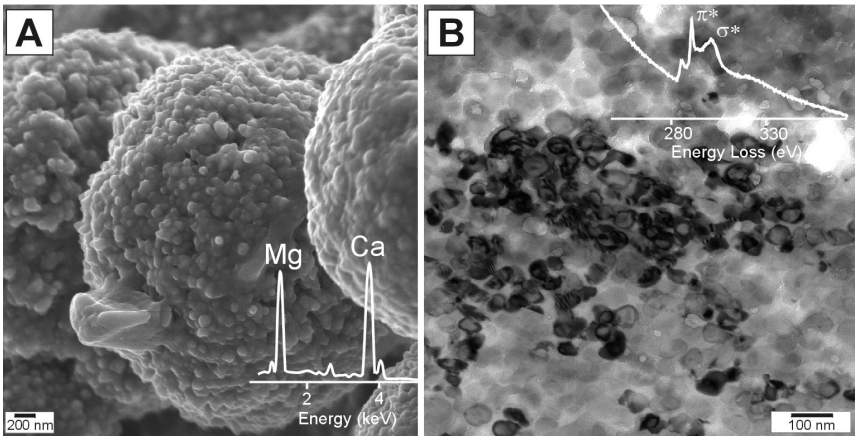

Figure 12. (A) SEM image and EDX spectra of Mg-kutnahorite spherulites obtained from gel growth inorganic precipitation experiments. They are formed by aggregation of rounded growth units, less than 100 nm in size. (B) TEM image (ESI mode) of Ca-Mg carbonate nanoparticles forming Mg-kutnahorites. The two main C K edge peaks in the EELS spectrum of the nanoparticles correspond to π* and σ* antibonding molecular orbitals of CO_3^{2-} cluster (peaks at 290.2 and 301.3 eV respectively [25]). Less intense C K edge peaks from amorphous carbon coating appears also superposed.

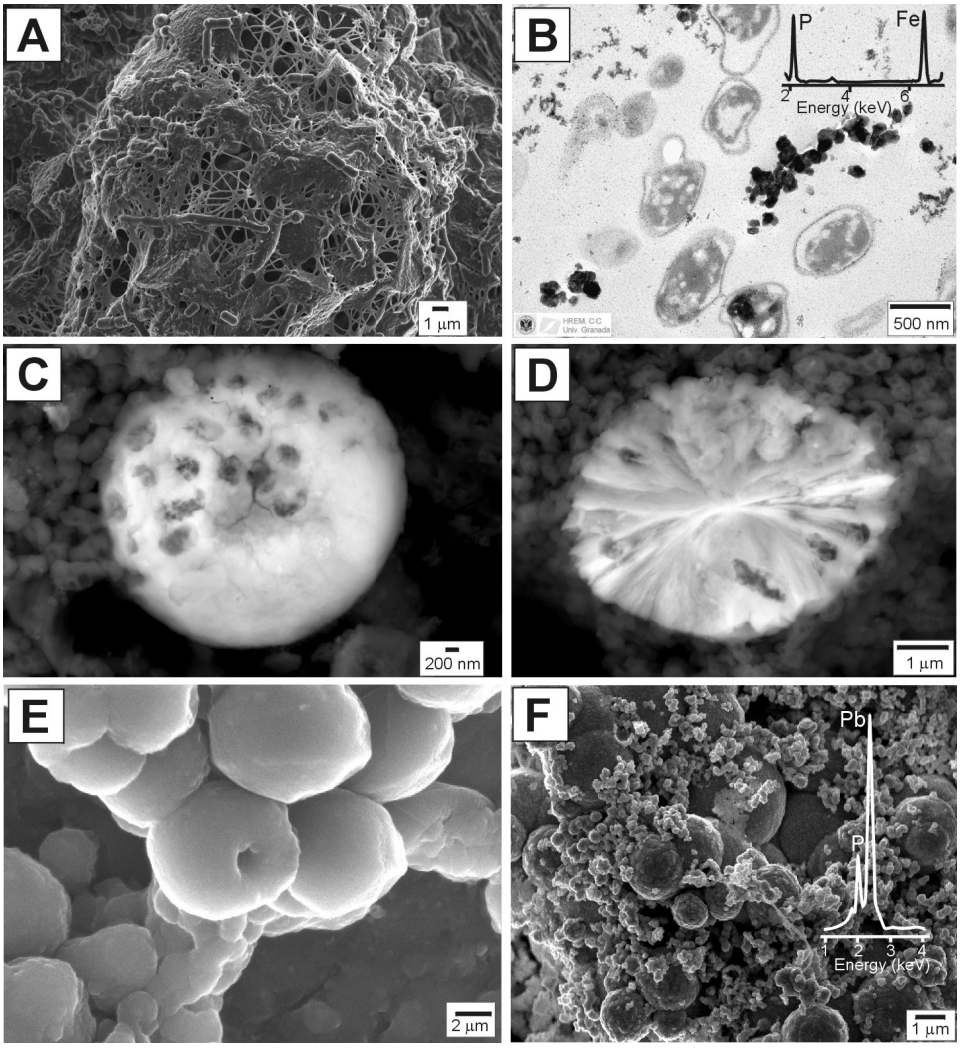

Figure 13. SEM and TEM images of bacterially-mediated phosphate precipitates obtained from precipitation experiments with vinegar dregs. (A) Secondary electron image corresponding to early stages of mineralization of the vinegar dreg. (B) TEM image of bacteria surrounded by iron phosphate nanoparticles, formed at the initial stages of mineralization. (C) SEM image of a Fe-phosphate spherulite with voids of 200 nm of size. (D) View of a sectioned spherulite showing a radial growth pattern and a porous texture. (E) Secondary electron image of Fe-phosphate capsules with smooth surfaces. (F) Pb-phosphate spherulites of very different sizes surrounded by irregular clumps of smaller Pb-carbonate particles.

Bacterially-mediated precipitation experiments with $CaCl_2.6H_2O$ (50 mM), and supplemented with bicarbonate (50 mM $NaHCO_3$), resulted in the formation of calcite spherulites and sheaf-like crystals (Fig. 14A). The latter are elongated following the *c* axis of calcite crystals. They are

formed by aggregation of rounded nanoparticles, with sizes smaller than 50 nanometres, at their tips (Fig. 14B).

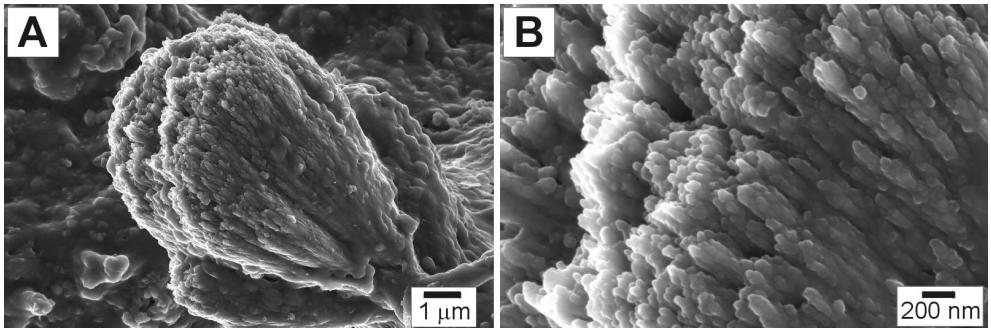

Figure 14. (A) Bacterially-mediated, shrub-like Ca-carbonate precipitate. (B) Close-up of (A), showing the parallel aggregate of calcite crystals elongated along the *c* axis. They grow by aggregation of rounded nanoparticles usually less than 50 nm in size.

4. Discussion

4.1. Kinetics constraints on crystal growth of carbonate and phosphate minerals

Metal phosphates and carbonates occurring in the studied natural samples and in the precipitates obtained from biotic and abiotic experiments develop complex crystal morphologies: from single crystals to crystalline aggregates forming dumbbells and spherulites. In some inorganic experiments, several tens of microns-sized polyhedral forms have been obtained directly (Fig. 11A). However, crystal growth features observed in most samples indicate that phosphates and carbonates here studied can be considered "mesocrystals".[26] These are superstructures formed by the aggregation of nanocrystal building units (Figs. 10E, 12 and 14) that are frequently associated with amorphous precursors (Figs. 1, 4, 5, 8, 9, 10E and 10F). A comparison between the morphology of abiotic and biotic precipitates may help to understand nucleation and crystal growth of new organic-inorganic hybrid materials that are crystallized by oriented aggregation of nanoparticles instead of by ion-by-ion or single molecule attachment. Actually, the occurrence of nanocrystalline particles and aggregation based morphologies within an organic matrix seems be key features of biomineralization.[13, 27]

Precipitation of calcium phosphate and carbonate nanoparticles on diverse substrates in relation to gelly-like substances may be the dominant mechanism of phosphate and carbonate formation in some geologic, microbially-mediated biosedimentary structures (Figs. 2-5)[7, 31] and in some calcified tissues (Figs. 6-8).[23, 24] In phosphate stromatolites, the authigenic clay and phosphate laminae within stromatolites are related to the formation of an extracellular, mucilaginous, bacterial gel, rich in polysaccharides at the living microbial mat.[7, 31] It has

been shown that gelly-like media favour the nucleation and the formation of clusters of nanocrystals within hydrogel networks.[27] High supersaturation occurring in gel media leads to the formation of assemblies of nanometer-sized crystalline particles that actually constitute the building blocks of larger crystalline aggregates. These textural features are less frequently formed in crystal-growth from diluted solutions.[28]

Spherulitic morphologies typically form at extremely high growth rates, and result from highly nonequilibrium processes operating both in solution and gel growth.[29] Siderite spherulites have been produced under high supersaturation in solution growth for some inorganic precipitation experiments (Figs. 10B, 10C, 10D and 10 F). In bacterially-mediated precipitation, spherulites of many carbonate and phosphate mineral can be precipitated (Figs. 13 and 14). In this case, the fast attachment of building blocks to the surface of the spherulites frequently preserves bacterial moulds and capsules, and voids are also very common (Figs. 13C, 13D, and 13E). Either obtained in biotic or abiotic experiments, all these spherulites and related morphologies are characterized by a radial texture of nanocrystal aggregates resulting from a geometrical selection process. In this way, fastest crystal-growth directions are perpendicular to the growing surface (Figs. 6, 10C, 10D, and 14). Honeycomb-like aggregates of small hexagonal apatite crystals of dental enamel (Fig. 6B) and equivalent parallel aggregates of prismatic phosphate crystals observed in phosphate stromatolites also result from competitive crystal growth processes.

The obtained carbonate and phosphate nanocrystals constitute a finely divided crystalline matter composed by particles that attach each others (Figs 4, 7, 8C, 8D, 9B, 9C and 12B). However, the aggregation of these nanoparticles is not related to atom-by-atom attachment, as they are still very large when compared to the atomic size scale. In nanometre-size crystals, the density of electronic energy levels, related to the energy of valence electrons responsible of the chemical bonds, varies smoothly between the atomic and bulk limits.[30] In very small nanocrystals the energy absorption spectra develop discrete features, similar to van der Waals or molecular crystals, where the bands in the solid are very narrow. Therefore, the interactions that allow the attachment of nanocrystals during the aggregation-based growth-process producing some of the crystal growth features here described must be very weak.

As shown in this work, and also described elsewhere, [7,31] apatite crystals of the authigenic laminae in phosphate stromatolites are usually surrounded by poorly crystalline smectites and Fe-Si-Al amorphous oxyhydroxides (Figs. 3, 4 and 5). These substances represent the fossil record of a mineralized extracellular mucilaginous bacterial gel that played the same role as bacterial organic matter in biotic laboratory experiments, and an equivalent role to that played by organic framework rich in collagen fibrils of dentine and bone. However, crystal growth features observed in authigenic phosphates (francolite) and smectitic clays of stromatolite laminae are not exclusively explained by the occurrence of gelly-like organic substances in a precursory microbial mat. In addition, the clay-rich material and related amorphous substances in phosphate stromatolites play an analogous role to that of gels in inorganic and biomediated experiments. In such media, bulk flow of a grain boundary fluid containing dissolved solutes does not occur. Within clay-rich media, fluid film is restricted to a monolayer of adsorbed molecules onto the clay particles. This suppresses convective and advective mass

transport and favours diffusion and the development of spherulitic instead of polyhedral morphologies (see next section). Therefore clayey material acts as a gel, and its occurrence favours the formation of amorphous precursors and nanocrystals of later precipitates. This is the case of francolite crystallization in phosphate stromatolites, which is preceded by the precipitation amorphous calcium phosphate, as suggested by Sánchez-Navas and Martín-Algarra.[7]

4.2. Considerations related to gel growth and structural control of habit in Mg-Ca carbonates

Gels and related substances are responsible for high supersaturation producing the crystal growth features observed in the solid porous media. High supersaturation gradients arise from the slow transport of the chemical species present in gel growth experiments, and the degree of supersaturation driving the crystallization depends on the diffusion gradient in solid porous media.[28] Hence, high growth rates are expected in porous media where the critical supersaturation for phosphate and carbonate minerals is reached more quickly than in solution growth.

Gel growth also explains why some elements like Mg are incorporated to the structure of calcite. A correlation between Mg-content in calcite and crystallinity may be deduced from the figure 11. Slow diffusive transport media, such as a clay-rich and water deficient environments or porous media, make the transport of reacting material from solution to those of growth be the rate-determining process. Transport properties in porous media controls on the incorporation of elements during the crystal growth.[32] To understand it, we may suppose that the partition coefficient between the concentration of magnesium in carbonate crystal and its concentration in bulk medium ($C^{Mg}_{crystal} / C^{Mg}_{medium}$) is less than 1. When carbonate crystal growth is diffusion controlled, the concentration of Mg at the crystal-medium interface rises above its concentration in the medium. If the partition coefficient remains constant, the Mg concentration in the carbonate increases due to the slower diffusion rate and, in the limit, it is equal to the concentration of Mg in the medium. It makes that the effective partition coefficient $C^{Mg}_{crystal} / C^{Mg}_{medium}$ equals 1 and, therefore, most of the Mg of the medium is incorporated into the structure of the rhombohedral carbonate.

Crystal chemical substitution of Mg for Ca within the structure of rhombohedral carbonates decreases crystallinity, stabilizes nanocrystals and favours an aggregation-based crystal growth. The different size of the cations involved (Ca^{2+} and Mg^{2+}) distorts the calcite crystal lattice. Of these two cations the Mg^{2+} ion has the smallest ionic radius. The lattice contraction due to the substitution of Mg for Ca is evidenced by the displacement of the (104) peak in XRD patterns (Fig. 11). The $d_{(104)}$-spacing and lattice constants of Mg-calcite are shorter than those of calcite, being the *c* axis the most affected by the incorporation of Mg.[33] This lattice contraction causes the CO_3^{2-} anions layers to be pulled closer together along the *c*-axis and produces a lattice deformation around Mg atoms. The incorporation of Mg into the crystal structure increases drastically the volume strain energy. This prevents reduction in free energy for nucleation with size increase and, therefore, further growth of nanocrystals. In addition, lattice contraction also stabilizes attractive interactions among nanocrystals. Lattice contrac-

tion carries out nonbonded repulsion between CO_3^{2-} anions within the structure of the rhomboedral carbonates. The more the distance between CO_3^{2-} anions decreases because of the incorporation of the small Mg cation into the structure of calcite, the more repulsion increases. The increase of nonbonded repulsion makes valence electrons feel less potential wells.[34,35] In the case of carbonates, electrons feel less the potential of the oxygen nuclei within CO_3^{2-} anions. The decrease of electron binding energy in O atoms increases oxygen polarizability. The improvement of the so-called polarization, correlation, Van der Waals or long-range forces between CO_3^{2-} enhances nanocrystals attachment during the aggregation-based growth-process.

5. Conclusions

Crystal growth features in biogenic and abiotic carbonates and phosphates occurring in natural environments (phosphate stromatolites and calcified tissues -bone and teeth) and formed in laboratory experiments are described in this work.

Phosphate and carbonate minerals precipitated from abiotic and biotic experiments form commonly spherulites and related morphologies. In most cases they can be considered mesocrystals because, independent of their biotic or abiotic origin, they are superstructures formed by the aggregation of nanocrystal building units and appear associated with amorphous precursors. Parallel aggregates constituted by Ca-phosphate crystals are formed by competitive crystal growth processes and, together with amorphous Ca-phosphates, are observed in dentine and enamel as well as in phosphate stromatolites.

Gels in laboratory experiments, organic matrix in calcified tissues and equivalent clay-rich media in phosphate stromatolites favour diffusive transport and supersaturation of carbonate and phosphate minerals. Supersaturation is responsible for the development of spherulitic morphologies and the occurrence of nanometre-sized crystals and related amorphous substances. Gels also explain the incorporation of some elements as Mg to the structure of calcite.

Acknowledgements

We acknowledge support from grants CGL-2009-09249 (DGICYT, Spain) and P11-RNM-7067 of the Junta de Andalucía (Spain), and by the research group RNM-179 (Junta deAndalucía). We would like to thank María José Martínez Guerrero, Alicia González Segura, María del Mar Abad Ortega, Concepción Hernández, Isabel Guerra Tschuske and Juan de Dios Bueno (Centro de Instrumentación Científica-CIC, University of Granada) for guidance with SEM-EDX and TEM-AEM-EELS studies. Agustín Martín Rodríguez, José Suarez Valera, María Navas Moreno and Elena Beatriz Sánchez Martín significantly helped with laboratory precipitation experiments.

Author details

Antonio Sánchez-Navas[1], Agustín Martín-Algarra[2], Mónica Sánchez-Román[3], Concepción Jiménez-López[4], Fernando Nieto[1] and Antonio Ruiz-Bustos[1]

1 Departamento de Mineralogía y Petrología, Facultad de Ciencias, Universidad de Granada, Granada, Spain

2 Departamento de Estratigrafía y Paleontología, Facultad de Ciencias, Universidad de Granada, Granada, Spain

3 Centro de Astrobiología, INTA, Torrejón de Ardoz, Madrid, Spain

4 Departamento de Microbiologia, Facultad de Ciencias, Universidad de Granada, Granada, Spain

Instituto Andaluz de Ciencias de la Tierra. C.S.I.C., Armilla, Granada, Spain

References

[1] Capewell SG, Hefter G, May PM. Potentiometric investigation of the weak association of sodium and carbonate ions at 25 ºC. Journal of Solution Chemistry 1998; 27: 865-877.

[2] Benjamin MM. Water Chemistry. New York: McGraw-Hill; 2001.

[3] Broecker WS, Peng TS. Tracers in the Sea. New York: Lamont-Doherty Geological Observatory; 1982.

[4] Bonucci E. Biological calcification. Berlin: Springer-Verlag; 2007.

[5] Cowan J, Weintritt D. Water formed scale deposits. Houston: Gulf Publ. Co.; 1976.

[6] Allwood AC, Walter MR, Kamber BS, Marshall CP, Burch IW. Stromatolite reef from the Early Archaean era of Australia. Nature 2006; 441: 714-718.

[7] Sánchez Navas A, Martín Algarra A. Genesis of apatite in phosphate stromatolites. European Journal of Mineralogy 2001; 13: 361-376.

[8] Allen CC, Albert FG, Chafetz HS, Combie J, Graham CR, Kieft TL et al. Microscopic physical biomarkers in carbonate hot springs: implications in the search for life on Mars. Icarus 2000; 147: 49-67.

[9] McKay DS, Thomas-Keptra KL, Romanek CS, Gibson Jr EK, Vali H. Evaluating the evidence for past life on Mars. Science 1996; 274: 2123-2124.

[10] Allwood AC, Walter MR, Kamber BS, Marshall CP, Burch IW. Stromatolite reef from the Early Archaean era of Australia. Nature 2006; 441: 714-718.

[11] Chivas AR, Torgersen T, Polach HA. Growth rates and Holocene development of stromatolites from Shark Bay, Western Australia. Australian Journal of Earth Science 1990; 37, 113-121.

[12] Walter MR, Golubic S, Preiss WV. Recent stromatolites from hydromagnesite and aragonite depositing lakes near the Coorong Lagoon, South Australia. Journal of Sedimentary Research 1973; 43: 1021-1030.

[13] Rivadeneyra MA, Martín-Algarra A, Sánchez-Román M, Sánchez-Navas A, Martín-Ramos D. Amorphous Ca-phosphate precursors for Ca-carbonate biominerals mediated by Chromohalobacter marismortui. The ISME Journal 2010; 4: 922-932.

[14] Buczybnski C, Chafetz HS. Habit of bacterially induced precipitates of calcium carbonate and the influence of medium viscosity on mineralogy. Journal of Sedimentary Petrolology 1991; 61, 226-233.

[15] Ehrlich HL. Geomicrobiology (4th edn.). New York: Marcel Dekker; 2002.

[16] Sánchez-Navas A, Martín-Algarra A, Rivadeneyra MA, Melchor S, Martín Ramos JD. Crystal-Growth Behavior in Ca–Mg Carbonate Bacterial Spherulites. Crystal Growth and Design 2009; 9: 2690-2699.

[17] Sunagawa I. Morpholgy of Crystals. Tokyo: Terra Scientific Publishing Company; 1987.

[18] Checa González A, Sánchez-Navas A, Rodríguez-Navarro A. Crystal growth in the foliated aragonite of monoplacophorans (Mollusca). Crystal Growth and Design 2009; 9: 4574-4580.

[19] Martín-Ramos J.D., Díaz-Hernández J.L., Cambeses A., Scarrow J.H., López-Galindo A. Pathways for Quantitative Analysis by X-Ray Diffraction. In: Aydinalp C. (ed.) An Introduction to the Study of Mineralogy. Rijeka: InTech; 2012. http://www.intechopen.com/articles/show/title/pathways-for-quantitative-analysis-by-x-ray-diffraction (accessed 20 July 2012).

[20] Vali H, Koster HM. Expanding behaviour, structural disorder, regular and random irregular interstratification of 2–1 layer-silicates studied by high-resolution images of transmission electron-microscopy. Clay Minerals 1986; 21: 827-859.

[21] Jarvis I. Sedimentology, geochemistry and origin of phosphatic chalks: the Upper Cretaceous deposits of NW Europe. Sedimentology 1992; 39: 55-97.

[22] De Vrind-de-Jong E.W., de Vrind J.P.M. Algal deposition of carbonates and silicates. In. Banfield J.F., Nealson K.H. (eds.) Geomicrobiology: Interactions between Microbes and Minerals. Reviews in Mineralogy: Mineralogical Society of America; 1997. p267-307.

[23] Landis WJ, Hodgens KJ, Arena J, Song MJ, McEwen BF. Structural Relations Between Collagen and Mineral in Bone as Determined by High Voltage Electron Microscopic Tomography. Microscopy Research and Technology 1996; 33: 192-202.

[24] Ziv V, Sabanay I, Arad T, Traub W, Weiner S. Transitional structures in lamellar bone. Microscopy Research and Technology 1996; 33: 203-213.

[25] Garvie LAG, Graven AG, Brydson R. Use of electron-energy loss near-edge fine structure in the study of minerals. American Mineralogist 1994; 79: 411-425.

[26] Cölfen H, Antonietti M. Mesocrystals: Inorganic Superstructures Made by Highly Parallel Crystallization and Controlled Alignment. Angewandte Chemie International Edition 2005; 44: 5576-5591.

[27] Grassmann O, Neder RB, Putnis A, Löbmann P. Biomimetic control of crystal assembly by growth in an organic hydrogel network. American Mineralogist 2003; 88: 647-652.

[28] Putnis A, Prieto M, Fernández-Díaz L. Fluid supersaturation and crystallization in porous media. Geological Magazine 1995; 132: 1-13.

[29] Gránásy L, Pusztai T, Tegze G, Warren JA, Douglas JF. Growth and form of spherulites. Physical Review E 2005; 72 (011605): 1-15.

[30] Alivisatos AP. Nanocrystals: building blocks for modern materials design. Endeavour 1997; 21(2): 56-60.

[31] Sánchez-Navas A, Martín-Algarra A, Nieto F. Bacterially-mediated authigenesis of clays in phosphate stromatolites. Sedimentology 1998; 45: 519-533.

[32] Henderson P. Inorganic geochemistry. Oxford: Pergamon Press; 1986.

[33] Goldsmith JR, Graf DL. Lattice constants and composition of the calcium magnesium carbonates. American Mineralogist 1961; 46: 453-457.

[34] Bader RFW, Preston HJT. A critique of Pauli repulsions and molecular geometry. Canadian Journal of Chemistry 1966; 44: 1131-1145.

[35] Bader RFW. Pauli repulsions exist only in the eye of the beholder. Chemistry European Journal 2006; 12: 2896-2901.